DETECTION OF CRUSTAL MOVEMENTS DUE TO AFTERSHOCKS OF THE 2011 TOHOKU, JAPAN EARTHQUAKE FROM TERRASAR-X IMAGES

Wen LIU[a], Fumio YAMAZAKI[b], Takashi NONAKA[c], Tadashi SASAGAWA[c]

[a] PhD. Student, Department of Urban Environment Systems, Chiba University; JSPS research fellow
1-33 Yayoi-chou, Inake-ku, Chiba, Japan;
Tel: +81-43-290-3528; E-mail: wen_liu@graduate.chiba-u.jp

[b] Professor, Department of Urban Environment Systems, Chiba University
1-33 Yayoi-chou, Inake-ku, Chiba, Japan;
Tel: +81-43-290-3557; E-mail: yamazaki@tu.chiba-u.ac.jp

[c] Satellite Business Division, PASCO
Meguro Building Annex, 2-8-10 Higashiyama, Meguro-ku, Tokyo 153-0043, Japan;
Tel: +81-3-4570-3065

Abstract: After the March 11, 2011 Tohoku, Japan earthquake (Mw9.0), numerous aftershocks and induced events occurred in the source region of the main shock and its outside areas. One of the most damaging induced earthquakes with Mw7.1 occurred in Fukushima prefecture on April 11, 2011. This event caused the numerous fault scarps, with a maximum displacement of 2.3 m. In this study, two temporal TerraSAR-X images were used to detect the crustal movements in Fukushima region due to these events by two different methods. Firstly, the interferometric (InSAR) analysis was carried out to detect the crustal movement to the radar sensor direction. Due to the temporal decorrelation, InSAR fringes could be obtained in a small part of the area. Secondly, the building-based pixel-offset method, proposed by the present authors, was applied to the SAR intensity images. 2D movements were detected for a half of the study area. Finally, the results were compared with the recorded displacements from GPS ground stations. The difference between the movements detected by the second method and the records was less than 0.3 m, showing high accuracy of our method.

INTRODUCTION

The Mw9.0 Tohoku Earthquake occurred on March 11, 2011, off the Pacific coast of the northeastern (Tohoku) Japan, caused gigantic tsunamis, resulting in widespread devastation. It also caused large crustal movements over a wide area with maximums of 5.3 m to the horizontal (southeast) and 1.2 m to the vertical (downward) directions. Due to this event, Japan had experienced over 900 aftershocks by September 7, 2012, with about 60 aftershocks being over magnitude 6.0 and three over magnitude 7.0. The Fukushima Earthquake with Mw7.1 occurred on April 11, 2011was one of the most damaging induced earthquakes. Since it was caused by an inland active fault at a shallow depth (13 km), severe shaking was felt in the large area. The epicenter was located at 37.01° N, 140.48° E. It caused the numerous fault scarps, with a maximum displacement of 2.3 m.

Two methods have normally been used to detect crustal movements from remote sensing images in the past studies. The first one is interferometric analysis of synthetic aperture radar (InSAR) (Zebker, 2000). Several studies have been conducted to detect displacements due to earthquakes based on differential SAR interferometry (DInSAR) (Stramondo *et al.*, 2002; Chini *et al.*, 2010). However, depending on vegetation and temporal decorrelation, InSAR may not always be able to measure ubiquitous deformation at a large scale. In additional, InSAR can only detect the movements to the slant range direction. The second method is the pixel-offset method, which can be applied to both SAR and optical images (Bürgmann *et al.*, 2000; Michel *et al.*, 1999; Tobita *et al.*, 2006). In the 2011 Tohoku earthquake, the extent of crustal movements was much larger than the SAR imaging area. Due to the absence of the accurate geocoding information, it was difficult to detect the absolute displacement using the previous methods. The high-accuracy georeferenced product, however, has become available recently due to the improvement of SAR sensors and thus an improved pixel-offset method was proposed by the present authors to estimate the absolute ground displacements even in the case of large-scale tectonic movements (Liu and Yamazaki, 2012). In our previous research, the proposed method has been tested on 4 temporal TerraSAR-X (TSX) images along the Sendai coast and the result was found to be highly accurate through the comparison with GPS recordings.

In this study, two TSX data taken before and after the Fukushima Earthquake on April 11, 2011 were used to detect crustal movements by both the InSAR analysis and the our pixel-offset method. The results from the two methods were compared and discussed. The accuracy was demonstrated by comparing the detected displacements with those from the GPS ground station records.

THE 4.11 FUKUSHIMA EARTHQUAKE AND FIELD SURVEY

The Fukushima earthquake was an intraplate (crustal) earthquake. The oceanic Pacific Plate is subducting beneath the continental Okhotsk (North American) Plate, on which most of the Tohoku region is situated. This earthquake occurred in the vicinity of the Idosawa Fault, which is a shallow crustal fault near Tabito, Iwaki City, Fukushima Prefecture. The general vertical displacements between 0.8 to 1.5 m have been revealed by ground surveys. The segments of the Idosawa Fault associated with this surface rupture were classified as the "Shionohira Fault" in 2011 (Kelson *et al.*, 2012).

The study area was focused on the coastal zone of Fukushima Prefecture as shown in Figure 1(a). An InSAR analysis was carried out for the ALOS/PALSAR images on March 3 and April 18, 2011 by the Geospatial Information Authortiy of Japan (GSI, 2011). The result was cited and shown in Figure 2(a). According to the GPS Earth Observation Network System (GEONET) by the GSI, the whole target area moved to the east direction after the mainshock, away from the PALSAR sensor in the ascending path. However, localized significant displacements were confirmed around Yunotake Fault, Shinohara Fault and Idosawa Fault, which were caused by the aftershocks. InSAR analysis of PALSAR images is, in general, an efficient way to grasp the overall trend of crustal movements within an imaging area.

A filed survey around Shionohira Fault was carried out by the present authors on June 18, 2012, more than one year after the Fukushima earthquake. The root of the filed survey is shown in Figure 2(b). We started from Nakoso, Iwaki City, along the prefectural road No. 71. Although most of the fault ruptures became indistinguishable after one year due to vegetation, there were four significant surface ruptures were observed by this field survey. Since Shionohira Fault crosses the route 71, the first fault could be found easily. The repair construction of the road was almost completed, as shown in the first picture in Figure 2(c). There was about 20 cm displacement still remaining between the north and south sides of the Fault. The second location was also on the route 71. The reconstruction was carrying out. More than 40 cm displacement was observed in this location. The third and fourth locations were far away from the route 71 in the mountain area. More than 60 cm displacements were confirmed at the both locations. According to these surface ruptures, the direction of Shionohira Fault could be easily seen as running from the southeast to the northwest.

TEERASAR-X DATA

Two temporal TSX images taken before and after the Fukushima earthquake are shown in Figure 1(b-c), which we used for detecting crustal movements. The TSX images included the epicenter of the earthquake and six GPS ground stations, which are named Fukushima-kawauchi, Takine, Iwaki-3, Iwaki, Iwaki-2 and Iwaki-4 from the north to the south, respectively. The pre-event image was taken on March 13, 2011 (UTC), while the post-event one was taken on September 4, 2011. Since the both images were taken after the mainshock, the crustal movements caused by the Tohoku earthquake were not included in this study. Two images were captured with HH polarization and in the descending path. They have the same incident angle 37.4° at the center of the images. Since the images were acquired in the StripMap mode, the original resolutions were 3.30 m in the azimuth and 1.94 m in the range directions.

Both Enhanced Ellipsoid Corrected (EEC) and Single-look Slant-range Complex (SSC) products were used in this study. The SSC product includes both phase and amplitude information, which are necessary for the InSAR analysis. The EEC product was a topographically corrected multi-look intensity image, where the image distortion caused by a variable terrain height was compensated using a 90 m resolution SRTM DEM. The products were provided in the form projected to a WGS-84 reference ellipsoid with a resampled square pixel size of 1.25 m. Since the accuracy of the proposed pixel-offset method depends on the geocoding accuracy of TSX images, the geocoded standard EEC products were used, instead of the intensity images processed from the SSC products.

Two preprocessing approaches were applied to the EEC products before extracting crustal movements. First, the two TSX intensity images were transformed to a Sigma Naught (σ^0) value, which represents the radar reflectivity per unit area in the ground range. An Enhanced Lee filter (Lopes *et al.*, 1990) was then applied to the original SAR images to reduce the speckle noise. To minimize any loss of information included in the intensity images, the window size of the filter was set as 3×3 pixels. The pixel localization corrected by the GPS orbit determination was used directly in this study. According to the product specification document (Eineder *et al.*, 2010), the pixel
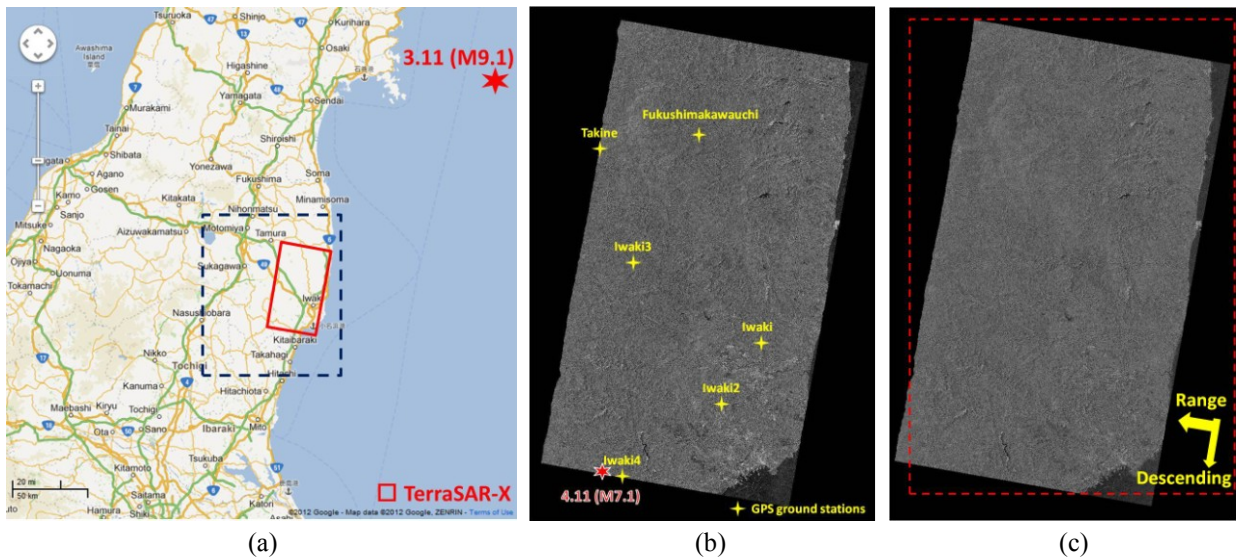
Figure 1: Study area along the Pacific coast of Tohoku, Japan (a) including six GPS ground stations; the pre-event TSX image taken on March 14 (b) and the post-event images taken on September 5 (c), 2011 (local time).
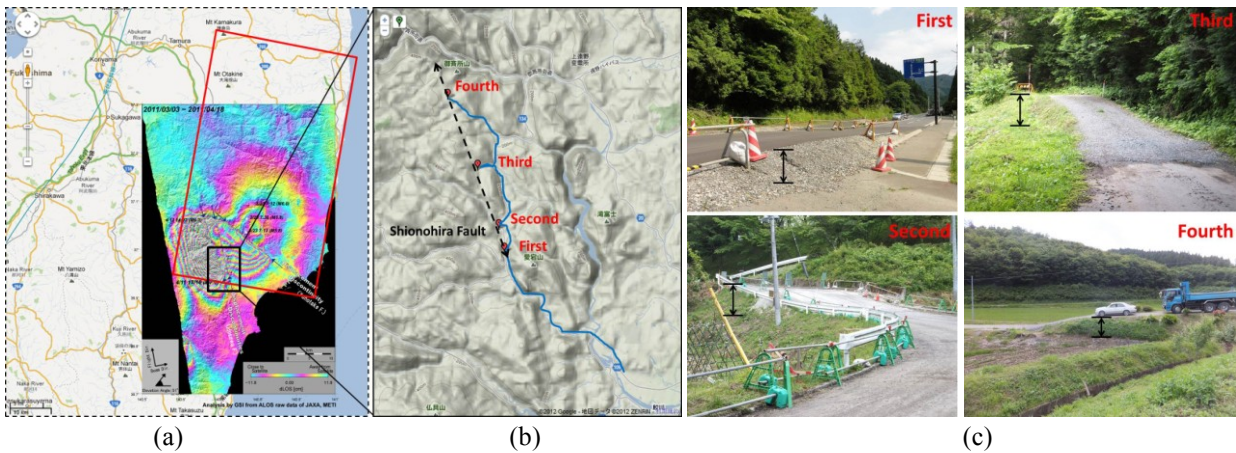

Figure 2: Interferogram of ALOS/PALSAR by GSI (a) on a close-up area of Figure 1(a); the field survey route and picture locations (b); ground pictures of the observable surface rupture (c)

localization accuracy of the EEC products depends on the orbit and the DEM used. Since the orbit type of our TSX images was "Science", their required orbit accuracy is within 20 cm, but actual data showed better than 10 cm accuracy (Wermuth *et al.*, 2009).

INTERFEROMETRIC ANALYSIS

An InSAR analysis was applied to the SSC products of the TSX images using *SARscape* software (SARscape, 2012) to detect the crustal movement. Firstly, an initial InSAR result was obtained using the two SSC TSX images. Then a 30 m resolution ASTER Global Digital Elevation Model (ASTER GDEM) was introduced to remove elevation effects from the initial result. Orbital fringes and noises were removed by a Goldstein filter. Finally, the geocoded coherence image was obtained and shown in Figure 3(a) by a rainbow color.

Due to the short wavelength of X-band SAR, the coherence in forest areas is very low. Since more than half of the target area was mountainous covered by vegetation, InSAR fringe could not be detected in these areas. In additionally, the 6 months time lag between the two images also caused low coherence. As a result, the average value of the coherence for the two TSX images was about 0.25. From Figure 3(a), it can be confirmed that only parts of the urban area along the coastline show high coherence larger than 0.5. Thus, the crustal displacement of the whole area could not be calculated using this result.
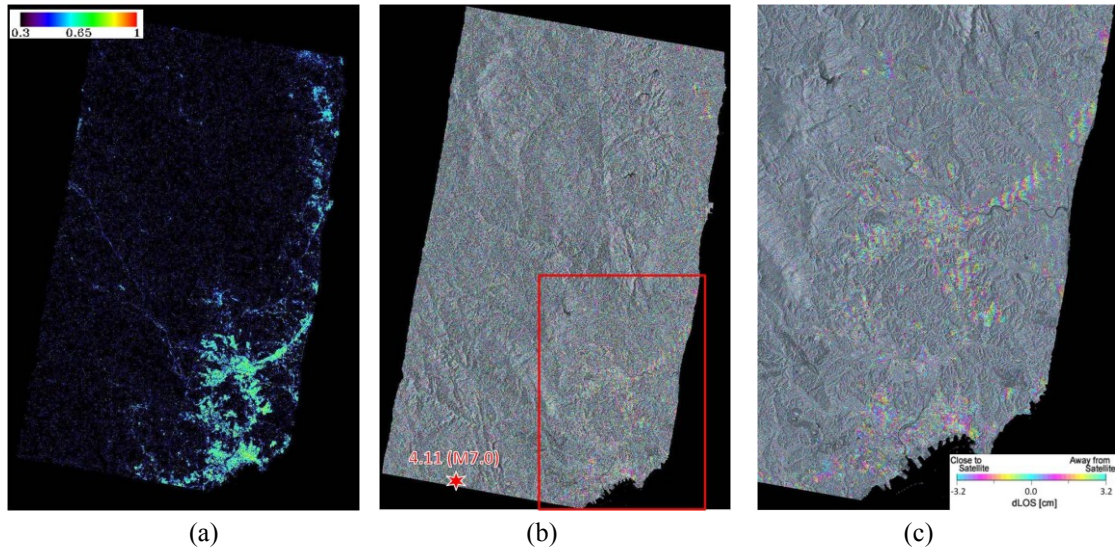
(a)	(b)	(c)

Figure 3: Coherence image obtained by InSAR analysis (a); composite of the detected interferogam on the intensity image (b) and a close-up of the red frame (c).

The composite InSAR result by overlapping InSAR fringes on the SAR intensity image is shown in Figure 3(b). The fringes, which represent the crustal movements, can be confirmed only in a part of the high coherence area. A close-up of the detected area is shown in Figure 3(c). A continuous fringe can be confirmed from the central part of Iwaki City to the northeast direction. According to the localized InSAR result, Iwaki City moved closer to the sensor direction, which is southeast in the descending path.

Although the overall trend of crustal movements in the target area could not be detected, the localized deformation was still confirmed from the result of the TSX images. Since one circle of interferogam in the TSX image represents the half length of the X-band wavelength, which is about 3.2 cm, the small displacement difficult to be seen from PALSAR with 23.6 cm wavelength could be observed from the TSX images. These small displacements are considered to be useful for locating buried pipeline damages.

PIXEL OFFSET METHOD

The crustal movements within the red frame in Figure 1(c) were extracted by the proposed pixel-offset method (Liu and Yamazaki, 2012) from the EEC products. Firstly, the whole target area was divided into a 2.5×2.5 km^2 mesh, shown in Figure 4(a). In each sub-area (2.5×2.5 km^2), solid buildings larger than 150 m^2 were extracted by a simple segmentation approach. The threshold value of the backscattering intensity used in segmentation was set as -2.5 dB, which means the pixels of larger than -2.5 dB were grouped as a building object. A color composite of the pre- and post-event TSX images in the sub-area including Iwaki-2 GPS station is shown in Figure 4(b), and the color composite of the extracted buildings is shown in Figure 4(c).

Then the non-changed buildings were extracted by comparing the building locations in the two building images. If a solid building exists in the post-event image around the location of a target building in the pre-event image within 5 pixels, the target building is regarded as non-changed. The displacement of a non-changed building between the two TSX intensity images was calculated by an area correlation method. To improve the accuracy, the TSX images surrounding non-changed structures were resampled to 0.25 m/pixel by cubic convolution to have 1/5 of the original pixel size. Thus, the shift of building shapes could be detected at a sub-pixel level. A target area was selected from the pre-event intensity image at the location of a non-changed building object. Then a search area, which surrounds the target area and exceeds it in size, was selected in the post-event intensity image. The target area was overlaid with the search area and was shifted within it. In each shift, a similarity index was calculated. The similarity matrix contained the values of the statistical comparison between the target and search areas. The maximum value in the matrix was determined as the correlation coefficient of the building, and the location of the maximum value was considered as the final offset of the target in the search area.
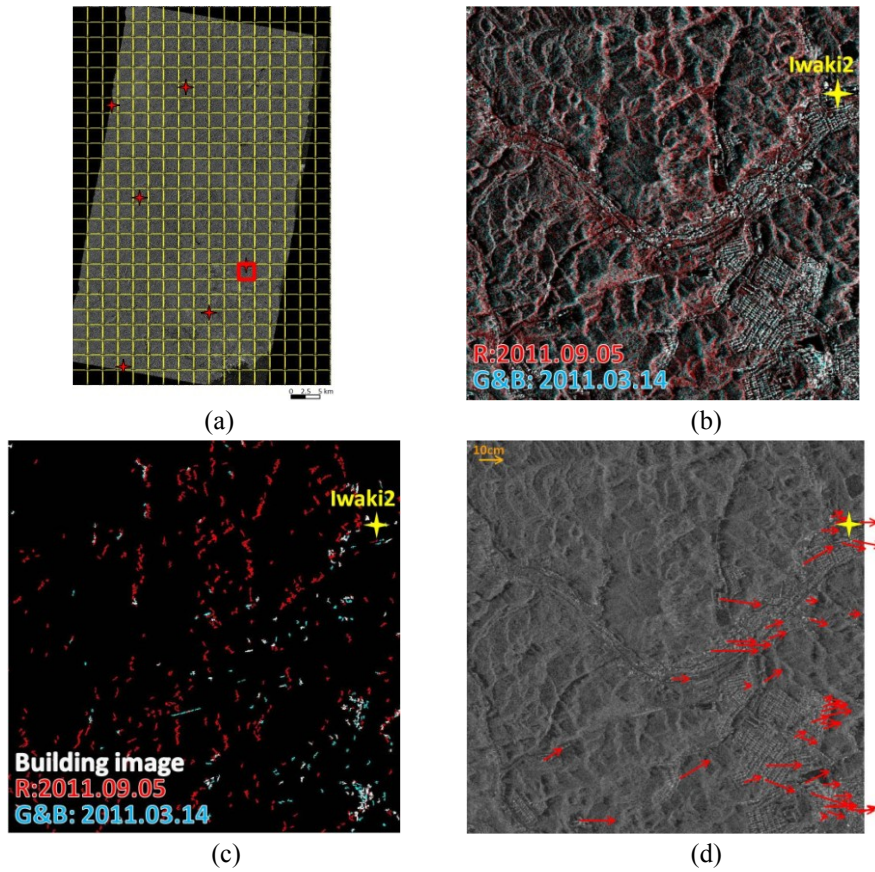
(a)

(b)

(c)

(d)

Figure 4: The SAR intensity image divided into a 2.5 km square mesh (a); a color composite of the pre- and the post-event TSX images in the sub-area including Iwaki-2 GPS station (b); the color composite of the extracted building images (c); and the detected displacements for non-changed buildings.
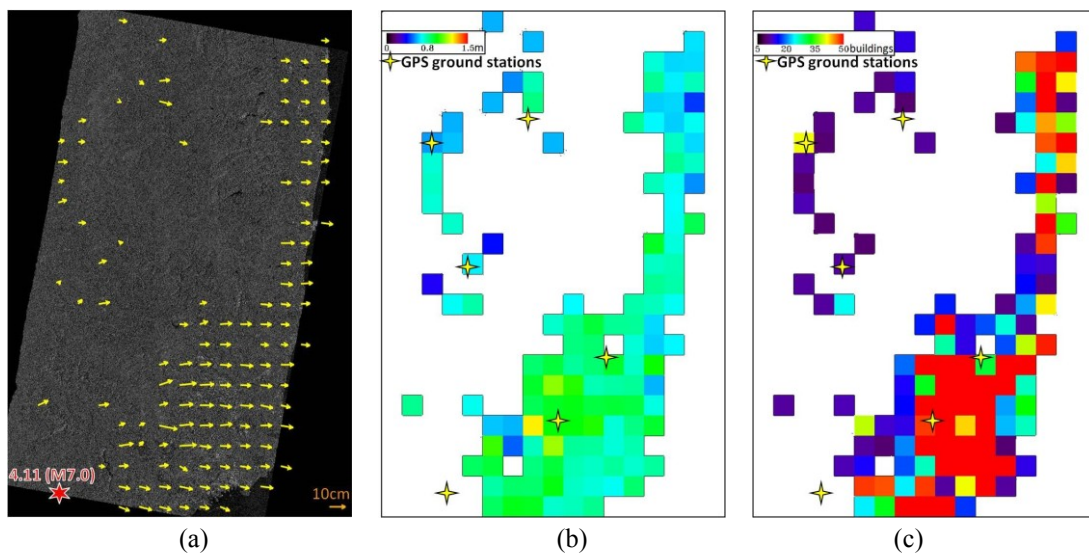

(a)

(b)

(c)

Figure 5: Detected displacement vectors in each sub-area overlapping on the pre-event TSX intensity image (a); the displacement amplitude shown in rainbow color (b); and the number of buildings used in each sub-area (c).

When the correlation coefficient of a non-changed building in the two TSX image was larger than 0.8, the detected displacement was counted as valid data. The movements of 29 non-changed buildings were detected in the Iwaki-2 sub-area, and shown in Figure 4(d). Although several displacements were distributed to different directions due to the sloping ground, the standard deviations to the east and north directions were both around 0.5 m. Finally, the average value of these movements was calculated and considered as the crustal movement in the Iwaki-2 sub-area, which were 0.87 m to the east and 0.09 m to the north directions.

The crustal movements in the whole area were detected in the same way. To ensure the reliability of the results, only a sub-area containing more than 5 building displacements was counted as valid one. Since the displacements were calculated from the location of buildings, the proposed method could not be applied to mountainous areas without buildings. The movements from 127 sub-areas were detected, and they are shown in Figure 5(a). The displacements of four sub-areas including GPS stations were detected. Two sub-areas including Fukushima-kawauchi and Iwaki-4 GPS stations could not be detected due to small number of buildings. The detected crustal movements in the four GPS sub-areas and the movements in neighboring sub-areas for the two GPS stations were shown in Table 1. A comparison of the detected movements in the table shows that the largest movement occurred around Iwaki-2 GPS station. The westward movement, the opposite direction with the other areas, was detected around Iwaki-4 station, located on the southwest side of Shinonohira Fault.

The displacement amplitude is shown in Figure 5(b) by a rainbow color. The largest detected movement was 1.23 m with 1.1 m to the east and 0.23 m to the north directions. The number of displacements detected in each sub-area is shown in Figure 5(c). The more number the detected displacements were, the more reliable the obtained result became. It was confirmed that several crustal movements that were directed to different directions with the surrounding sub-areas in Figure 5(a) were the sub-areas with small numbers of detected displacements in Figure 5(c). However, the detect result became stable when the number of detected displacements were more than 10.

Table 1: Comparison of detected crustal movements in six sub-areas surrounding the GPS stations by the proposed method and the GPS records (unit: meter). * indicates the result estimated from a nearby sub-area

	Fukushima-kawauchi*		Takine		Iwaki-3		Iwaki		Iwaki-2		Iwaki-4*	
	East	North	East	North	East	North	East	North	East	North	East	North
GPS record	0.41	-0.08	0.40	-0.06	0.38	-0.01	0.52	-0.07	0.74	-0.02	-0.43	0.30
Pixel offset	0.46	0.14	0.38	-0.08	0.46	-0.18	0.66	0.04	0.87	-0.09	-0.29	0.07
Difference	0.05	0.22	-0.02	-0.02	0.08	-0.17	0.14	0.11	0.13	-0.07	0.14	-0.23

VERIFICATION OF THE RESULTS

To verify the accuracy of the detected movements by the two methods, the crustal movement data from the GPS stations were introduced. The surface displacement is a vector in the three-dimensional (3D) space with three components, D_E, D_N, and D_Z, to the east, north, and vertical directions, respectively. The relationship between an actual crustal movement and its shift in a SAR image is shown in Figure 6.

The result of InSAR analysis can only detect the movement to the slant range. The 3D movements (D) can be converted to a movement to the range direction (M_S) by the relationship shown in Equation (1).

$$M_S = \sin\theta \times (\cos\alpha \times D_E - \sin\alpha \times D_N) + \cos\theta \times D_Z \qquad (1)$$

where D is the actual movement to the east, north, and vertical directions; M is the shift in the SAR image; α is the heading angle clockwise from the north; and θ is the SAR incident angle.

It should be noted that the InSAR method can only provide the relative displacement within the target area. However, it was difficult to unwarp the InSAR interferogam obtained from the TSX images in this study due to the low coherence. The result could not be compared with the GPS station records.

The proposed pixel-offset method can detect a 2D movement from TSX intensity images to the east and north directions. The movement in the vertical direction is decomposed and transformed into the movements to the east and north directions. The relationship between an actual crustal movement and its 2D shift in a ground range SAR image is shown in Equation (2).

$$\begin{pmatrix} M_E \\ M_N \end{pmatrix} = \begin{pmatrix} 1 & 0 & -\cos\alpha/\tan\theta \\ 0 & 1 & \sin\alpha/\tan\theta \end{pmatrix} \begin{pmatrix} D_E \\ D_N \\ D_Z \end{pmatrix} \qquad (2)$$

where M_E and M_N are the shift in the SAR image to the east and north directions, respectively.
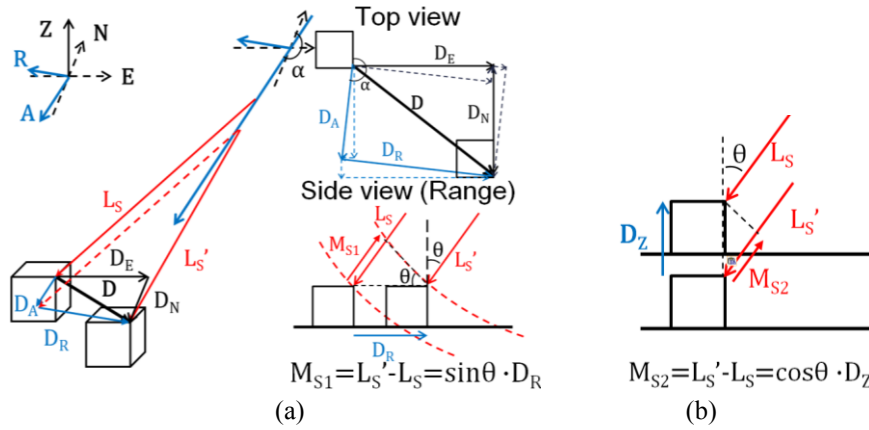
Figure 6: Schematic views of the horizontal (a) and vertical displacements (b) in a SAR image.

$$M_{S1} = L_S' - L_S = \sin\theta \cdot D_R \qquad\qquad M_{S2} = L_S' - L_S = \cos\theta \cdot D_Z$$
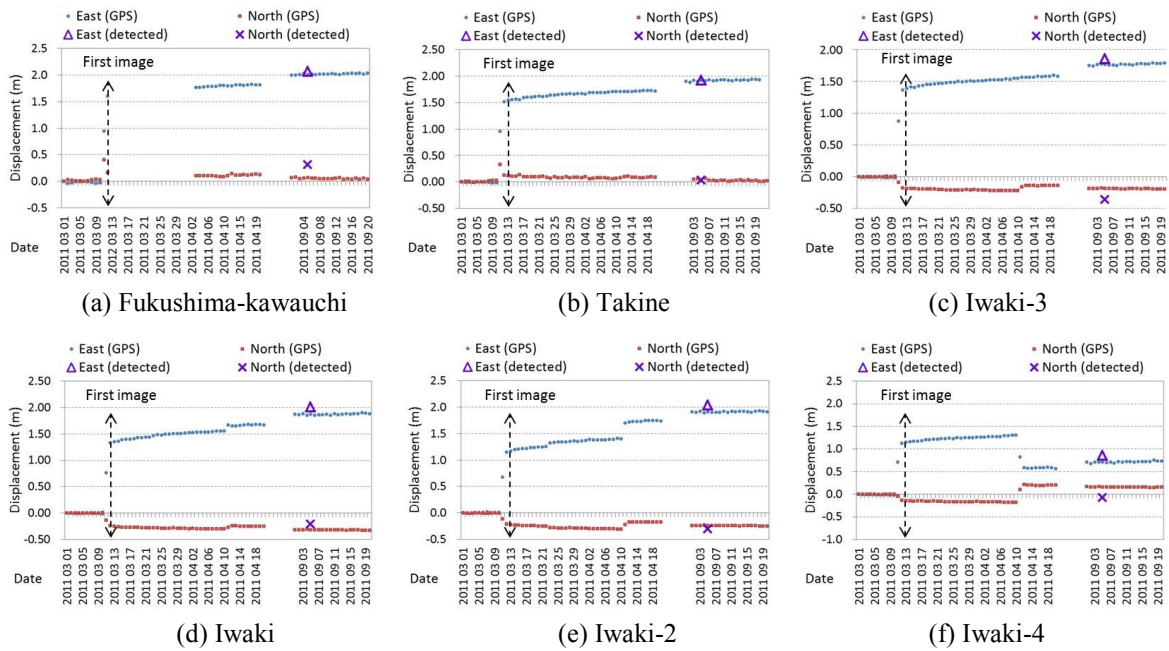

Figure 7: Comparison of movements converted from GPS data at Fukushima-kawauchi (a), Takine (b), Iwaki-3 (c), Iwaki (d), Iwaki-2 (e) and Iwaki-4 (f) ground control stations and the results detected in surrounding sub-areas.

The GPS recordings obtained at Fukushima-kawauchi, Takine and Iwaki1-4 stations from March 1 to April 20 and September 1 to 20, 2011, were converted using Equation (2) and are as shown in Figure 7. For the stations closer to the epicenter, more significant movements caused by the 11 April 2011 Fukushima Earthquake could be seen. The records of Iwaki-4 station exhibits a significant converse movement on April 11, due to the surface rupture of Shinonohira Fault. Since Iwaki-2 station is located close to the epicenter of the earthquake on March 23, 2011, the movements caused by Yunotake Fault could be confirmed from the records. The displacements between March 13 and September 5, 2011 converted from the GPS records were calculated and shown in Table 1.

A comparison of the results detected around the GPS stations with the converted GPS recordings demonstrated a very high level of consistency. Since the detected results are the movements in the period from March 13 to September 5, 2011, the recorded values at the GPS stations on March 13 were superposed on the detected results to match the standard value on March 1, 2011. The averaged differences between the detected result and the GPS measurement were about 0.10 m to the east and 0.14 m to the north. The maximum difference was 0.30 m.

CONCLUSIONS

In this study, we applied an InSAR analysis and an improved pixel-offset method for detecting crustal movements due to the 11April 2011 Fukushima Earthquake from two temporal TerraSAR-X images. The crustal movements were estimated from these two methods. Due to the short wavelength of the X-band SAR and the long time-lag between the two SAR images, the coherence between the two SSC TSX image were very low. The InSAR analysis

could only detect the relative movements in parts of the urban area. Compared with the InSAR result from PALSAR images, the overall trend of the crustal movement within the target area was difficult to detect from the TSX images. However, InSAR for TSX images has higher sensibility in detecting localized small displacements, even smaller than 10 cm.

Since the proposed pixel-offset method focused on non-changed buildings, it also only works in the area including buildings. However, the proposed method can detect the absolute two-dimensional movements, and provided more information than one-directional result by the InSAR analysis. Although it is impossible to detect the actual 3D movement only from the descending pair, the six sub-areas surrounding GPS ground stations exhibited stable shifts of non-changed buildings and they were close to the converted observed GPS data. Subpixel-based matching made it possible to detect movements with high accuracy, within 0.3 m which is 1/10 of its spatial resolution. However, the accuracy of our method depends on the location accuracy of the original SAR images and the elevation of the ground surface. It shows higher accuracy in a plain than in a sloping area. We will further test the proposed method for other earthquake events to verify its accuracy and applicability.

ACKNOWLEDGMENT

REFERENCES:

Bürgmann, R., P.A. Rosen, and E.J. Fielding, 2000. Synthetic Aperture Radar interferometry to measure earth's surface topography and its deformation, *Annual Reviews Earth and Planet Sciences*, 28, pp.169-209.

Chini, M., S. Atzori, E. Trasatti, C. Bignami, C. Kyriakopoulos, C. Tolomei, and S. Stramondo, 2010. The May 12, 2008, (Mw 7.9) Sichuan Earthquake (China): Multiframe ALOS-PALSAR DInSAR Analysis of Coseismic Deformation, *IEEE Geoscience and Remote Sensing Letters*, 7(2), pp. 266-270.

Eineder, M., T. Fritz, J. Mittermayer, A. Roth, E. Borner, H. Breit and B. Brautigam, 2010. TerraSAR-X Ground Segment Basic Product Specification Document. TX-GS-DD-3302, Issue 1.7, pp. 31-32.

Geospatial Information Authority of Japan (GSI), 2011. http://www.gsi.go.jp/cais/topic110425-index-e.html

Kelson, K.I., L.F. Harder, T, Kishida, and I. Ryder, 2011. Preliminary observations of surface fault rupture from the April 11, 2011 Mw6.6 Hamadoori Earthquake, Japan. *Geotechnical Extreme Events Reconnaissance*, No. GEER-025d.

Liu, W., and F. Yamazaki, 2012. Detection of crustal movement from TerraSAR-X intensity images. *IEEE Geoscience and Remote Sensing Letters*, DOI: 10.1109/LGRS.2012.2199076.

Lopes, A., R. Touzi, and E. Nezy, 1990. Adaptie speckle filters and scene heterogeneity. *IEEE Transactions on. Geoscience and Remote Sensing*, 28, pp. 992 -1000

Michel, R., J.-P. Avouac, and J. Taboury, 1999. Measuring ground displacements from SAR amplitude image: application to the Landers earthquake, *IEEE Geophysical Research Letters*, 26(27), pp. 875-878.

SARscape, 2009. http://www.exelisvis.com/ProductsServices/ENVI/SARscape.aspx

Stramondo, S. F., R. Cinti, M. Dragoni, S. Salvi, and S. Santini, 2002. The August 17, 1999 Izmit, Turkey, earthquake: Slip distribution from dislocation modeling of DInSAR and surface offset, *Annals of Geophysics*, 45(3/4), pp. 527-536..

Tobita, M., H. Suito, T. Imakiire, M. Kato, S. Fujiwara, and M. Murakami, 2006. Outline of vertical displacement of the 2004 and 2005 Sumatra earthquakes revealed by satellite radar imagery, *Earth Planets Space*, 48(1), pp. e1-e4.

Wermuth, M. A., Hauschild, O. Montenbruck, and A. Jäggi, 2009. TerraSAR-X Rapid and Precise Orbit Determination, In: *21st International Symposium on Space Flight Dynamics*, France.

Zebker, H.A., 2000. Studying the Earth with interferometric radar, *IEEE Computing in Science & Engineering*, 2(3), pp. 52-60.